Geophysical Research Letters

RESEARCH LETTER
10.1029/2025GL119305

Radar Estimates of Surfzone Dissipation Drive a Morphological Evolution Model

Florian Grossmann[1], **Michael Streßer**[2], **Britt Raubenheimer**[1], **and Steve Elgar**[1]

[1]Applied Ocean Physics and Engineering, Woods Hole Oceanographic Institution, Woods Hole, MA, USA, [2]Institute of Coastal Ocean Dynamics, Helmholtz-Zentrum Hereon, Geesthacht, Germany

Key Points:

- Radar-derived wave energy dissipation is used in sediment transport calculations for the first time
- Onshore and offshore sand bar migration is replicated with one set of calibration coefficients
- Including boundary layer effects and the vertical extent of suspended sediment improved results

Supporting Information:

Supporting Information may be found in the online version of this article.

Correspondence to:

F. Grossmann,
florian.grossmann@whoi.edu

Citation:

Grossmann, F., Streßer, M., Raubenheimer, B., & Elgar, S. (2026). Radar estimates of surfzone dissipation drive a morphological evolution model. *Geophysical Research Letters*, *53*, e2025GL119305. https://doi.org/10.1029/2025GL119305

Received 19 SEP 2025
Accepted 22 DEC 2025

Author Contributions:

Conceptualization: Florian Grossmann, Michael Streßer, Britt Raubenheimer, Steve Elgar
Data curation: Florian Grossmann, Michael Streßer, Britt Raubenheimer, Steve Elgar
Formal analysis: Florian Grossmann, Michael Streßer, Britt Raubenheimer, Steve Elgar
Funding acquisition: Florian Grossmann, Michael Streßer, Britt Raubenheimer, Steve Elgar
Investigation: Florian Grossmann, Michael Streßer, Britt Raubenheimer, Steve Elgar
Methodology: Florian Grossmann, Michael Streßer, Britt Raubenheimer, Steve Elgar

Abstract The dissipation of wave energy is important to nearshore circulation and beach profile evolution. Here, radar measurements of wave dissipation at the water surface across the surfzone are used to estimate water velocities and sediment transport in the lower water column to drive an energetics model for morphological change. The radar-driven model accurately simulates both the 25-m onshore and the 50-m offshore migration of a sand bar observed on an Atlantic Ocean beach with a single set of calibration coefficients. Similar to previous studies, wave asymmetry dominated during mild wave conditions when the bar migrated shoreward, and undertow dominated during energetic conditions when the bar migrated seaward. Model results were improved by accounting for both wave bottom boundary layer effects near the sand bar (especially during onshore migration) and the vertical extent of sediment suspension in the undertow transport (especially during offshore migration).

Plain Language Summary As ocean surface waves approach the coast they break in the shallow water of the surfzone, dissipating large amounts of energy, generating mean currents, and creating turbulence. Here, radar observations of dissipation and wave heights on an Atlantic Ocean beach are used to estimate the sediment transport driven by waves and currents. The transport terms are used in a model with one set of adjustable coefficients that predicts accurately the evolution of the seafloor as a sandbar migrates onshore and offshore. Consistent with previous studies, the results suggest onshore bar migration is dominated by waves that transport sediment shoreward in mild conditions, and that offshore migration is dominated by strong offshore-directed currents (undertow) that transport suspended sand seaward during energetic conditions. The model predictions are improved by considering near-bed effects near the crest of the sand bar during onshore migration and by including the vertical extent of suspended sediment during offshore migration.

1. Introduction

Nearly all ocean surface gravity wave energy that enters the nearshore is dissipated in the surfzone. Breaking transfers wave energy and momentum into the water column, generating currents and turbulence and suspending sediment, leading to morphological evolution, with important consequences for habitat, flood protection, tourism, and national security. Dissipation patterns are affected by the seafloor depth (Battjes & Janssen, 1978; Thornton & Guza, 1983), which determines the locations of depth-limited wave breaking (Miche, 1944) and roller propagation (the air-water mixture on the surface of breaking waves, Figure 1), the main nearshore dissipation processes (Deigaard, 1993; Stive & Wind, 1986; Svendsen, 1984, among others). Sandbars, alongshore ridges on the seabed (C. A. M. King & Williams, 1949; Wijnberg & Kroon, 2002, among others), initiate the breaking of onshore propagating waves through a rapid decrease in depth.

Simultaneously, wave breaking influences the sandbar position. During energetic conditions breaking waves suspend sediment and generate a time-mean offshore current (Aagaard et al., 1998; Gallagher et al., 1998; Thornton et al., 1996, among others), resulting in the offshore migration of sand bars (Dally & Dean, 1984; Dyhr-Nielsen & Sørensen, 1970, among others). During mild or moderate wave conditions when waves may shoal, but not necessarily break on the crest of the bar, sand bars migrate onshore owing to near-bed sediment transport driven by non-sinusoidal shaped nonlinear waves (Dubarbier et al., 2017; Grossmann, Hurther, Sánchez-Arcilla, & Alsina, 2023; Hoefel & Elgar, 2003; Rafati et al., 2021, among others). Both skewness (asymmetry about the horizontal axis) and asymmetry (asymmetry about the vertical axis) cause onshore transport (Dibajnia & Watanabe, 1992; Hoefel & Elgar, 2003; D. B. King, 1991, among others).

Project administration: Britt Raubenheimer, Steve Elgar
Resources: Florian Grossmann, Michael Streßer, Britt Raubenheimer, Steve Elgar
Software: Florian Grossmann, Michael Streßer, Britt Raubenheimer, Steve Elgar
Supervision: Britt Raubenheimer, Steve Elgar
Validation: Florian Grossmann, Michael Streßer, Britt Raubenheimer, Steve Elgar
Visualization: Florian Grossmann, Michael Streßer, Britt Raubenheimer, Steve Elgar
Writing – original draft: Florian Grossmann, Britt Raubenheimer, Steve Elgar
Writing – review & editing: Florian Grossmann, Michael Streßer, Britt Raubenheimer, Steve Elgar

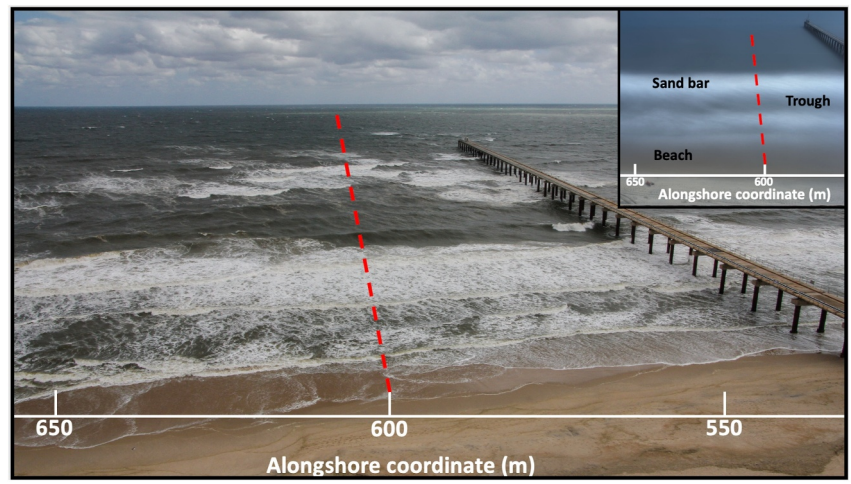

Figure 1. Photograph (not georectified) of the surfzone with ~1.5 m high incident waves. The approximate radar line of site is shown by the dashed-red line. The inset image in the upper-right corner is a 10-min time exposure of the surfzone, with white and dark bands indicating areas with waves that are breaking (on a shallow sand bar), not breaking (in the deeper tough onshore of the sand bar), and breaking (in the shallow water onshore of the bar close to the beach). The shore-based radar returns are used to estimate the corresponding dissipation.

Numerical models have skill simulating the offshore migration of sand bars during energetic conditions, but have been less successful in reproducing onshore bar migration (Gallagher et al., 1998; Roelvink & Stive, 1989; van Rijn et al., 2011, among others), at least partly owing to the difficulty of parameterizing nonlinear wave processes. Although some numerical models have skill simulating sandbar migration for a range of conditions (Ruessink et al., 2007), many models require different calibration coefficients for different sites or to replicate both onshore and offshore migration (Dubarbier et al., 2015; Fernández-Mora et al., 2015; Kroon et al., 2025; Rafati et al., 2021, among others).

The migration of sand bars has been tracked remotely using video (Holman & Stanley, 2007; Lippmann & Holman, 1990), satellite (Frugier et al., 2025), and radar data (Ruessink et al., 2002) with errors $\mathcal{O}$(10 m). These methods typically assume that sand bars are colocated with the surface foam from breaking waves. However, this assumption is not applicable during storms when waves are breaking over a wide cross-shore area, offshore, on top, and onshore of the sand bar, as well as during milder conditions when small waves do not break on the bar. Bathymetry inversion methods (Chernyshov et al., 2020; Holman et al., 2013; Lange et al., 2023, among others) typically use the dispersion relation to estimate water depths, including sand bars, from signals on the water surface. However, those methods tend to fail (errors of $\mathcal{O}$(1 m) in depth are common) for waves larger than about 1 m, possibly owing to errors in retrieval algorithms and neglect of nonlinear effects (Brodie et al., 2018).

Knowledge of the relationships between wave transformation and the generation of currents, turbulence, and sediment transport is critical to an improved understanding of the relationship between dissipation and morphological evolution. Remotely sensed roller quantities can be used to estimate wave dissipation, a forcing term in the nearshore momentum balance, as first demonstrated in a wave flume (Haller & Catalán, 2009) and later applied to field data (Díaz et al., 2018; Flores et al., 2016). These techniques typically rely on a conceptual roller model (Duncan, 1981), which relates roller geometry to dissipation, and can be applied to optical or thermal imagery (Carini et al., 2015; Haller & Catalán, 2009). However due to radar resolution limits, incoherent marine radar data must be combined with video to extract roller geometry (Catalán et al., 2011). Coherent radar systems provide an alternative by associating the observed Doppler velocity with dissipation via roller kinematics rather than geometry (Streßer et al., 2022).

Here, observations with coherent X-band radar (Horstmann et al., 2021; Streßer et al., 2022) provide quantitative estimates of breaking-wave dissipation across the surfzone on an Atlantic Ocean beach. The radar data are used to estimate wave heights, the associated water velocities, and the resulting sediment transport (described in the Text S1 in Supporting Information S1) to drive an energetics morphological change model (Bagnold, 1966; Bailard, 1981; Bowen, 1980; Dubarbier et al., 2015; Hoefel & Elgar, 2003; Hsu et al., 2006, among others). By

including wave bottom boundary layer effects near the sand bar and the vertical extent of sediment suspension in the undertow transport, the model simulates both the onshore and offshore bar migration with the same set of calibration coefficients.

2. Observations

A coherent-on-receive X-band radar (Horstmann et al., 2021) was deployed (Streßer et al., 2024, 2025) on a building deck overlooking the beach and surfzone at the US Army Corps of Engineers Field Research Facility (FRF) on the Outer Banks of North Carolina, near the town of Duck. The radar was located at $x = 34$, $y = 537$ m in the local FRF coordinate system and provided estimates of dissipation (Streßer et al., 2022) along the view direction of the antenna (Figure 1), which was aligned within a few degrees of shore normal at alongshore position ∼600 m (Figure 1), extending from 120 to 350 m in the cross-shore, similar to the bathymetric surveys along $y = 600$ m conducted with an amphibious vehicle (LARC). The surveys showed that a sandbar migrated both onshore and offshore during a 30-day period in October and November 2021 (surveyed positions of the sandbar crest are shown by the solid red circles in Figure 2a). Offshore (17-m water depth) significant wave heights $H_{s,0}$ ranged from 0.4 to 4.0 m (black curve in Figure 2a), periods from 5 to 12 s (Figure 2b), tidal water levels from −0.6 to 1.4 m relative to NAVD88 (similar to mean sea level, Figure 2c), and the cross-shore integrated roller energy estimated by the radar ranged from 0 to $10^5 \mathrm{kg} \cdot \mathrm{ms}^{-2}$ (Figure 2d).

During the first event, ON1 (10/13–10/16), wave heights were relatively low ($0.4 < H_{s,0} < 1.1$ m), and the bar migrated 25 m onshore in 1-m mean water depth over 3 days (Figures 2a and 3a). The second event, OFF (10/24–11/12), included two storms ($H_{s,0} > 2.0$ m) with 5 days of calm conditions in between (Figure 2a). Bathymetric surveys indicate 50 m overall offshore bar migration in 1- to 2-m water depth, with considerable erosion in the inner surfzone (Figure 3b compare solid-red with solid-black curves for $x < 200$ m) over 20 days. During the third event, ON2 (11/12–11/17), wave heights were relatively low ($0.4 < H_{s,0} < 1.2$ m), and the bar migrated 25 m onshore in 2-m water depth over 5 days (Figures 2a and 3c). The 3D bathymetric surveys (not shown) suggest that the bar migration events primarily were a cross-shore process, and that alongshore gradients in transport were small.

The radar records amplitude and phase of the received radiation (Horstmann et al., 2021), and measures the Doppler frequency shift induced by relative motions of Bragg resonant, centimeter scale waves that are the major source of ocean backscatter for vertically polarized X-band radars at moderate incidence (Valenzuela, 1978). At low-grazing incidence, additional scattering mechanisms become important (Frasier & McIntosh, 1996). Breaking-wave rollers increase both the backscatter intensity, and Doppler velocity (Catalán et al., 2014; Farquharson et al., 2005). Interpretation of the coherent radar signal at grazing incidence (Streßer et al., 2021) allows for measurements of the roller energy E_r and dissipation (Streßer et al., 2022) every 7.5 m along the cross-shore transect. The cross-shore integrated (over the surfzone) roller energy (Figure 2d) increases and decreases with the energy of offshore waves (Figure 2a).

The radar observations of the cross-shore evolution of E_r are used to estimate wave heights $H_s(x)$ along the surfzone transect (Streßer et al., 2022), requiring assumptions about the roller slope, β_s (taken here as 0.1 as typically used in the literature), and about other dissipation processes (Chen et al., 2024; Wu et al., 2025). Although there was no transect of in situ wave and current sensors across the surfzone to provide ground truth, the radar estimates of wave heights at the edge of the surfzone (∼4-m water depth, dashed-black curve in Figure 2a) are similar to incident waves heights observed with a buoy in 17-m water depth directly offshore of the field site (solid-black curve in Figure 2a), when incident waves were less than about 2 m (until about November 7 in Figure 2a). When incident waves were greater than about 2 m (e.g., November 8 in Figure 2a) the radar estimates of wave heights at the outer edge of the surfzone are lower than those observed in 17 m depth as expected owing to wave-breaking dissipation between 17 and 4 m depth. Thus, it is assumed the radar estimates of $H_s(x)$ also are reasonable. The model is initialized with observed bathymetry and uses radar estimates of roller energy, dissipation, and wave height to estimate hydrodynamic and sediment transport parameters (described below and in Text S1 in Supporting Information S1).

The energetics approach to predict sediment transport, $\hat{Q}$ (Bagnold, 1966; Bailard, 1981; Bowen, 1980) consists of several terms, given by

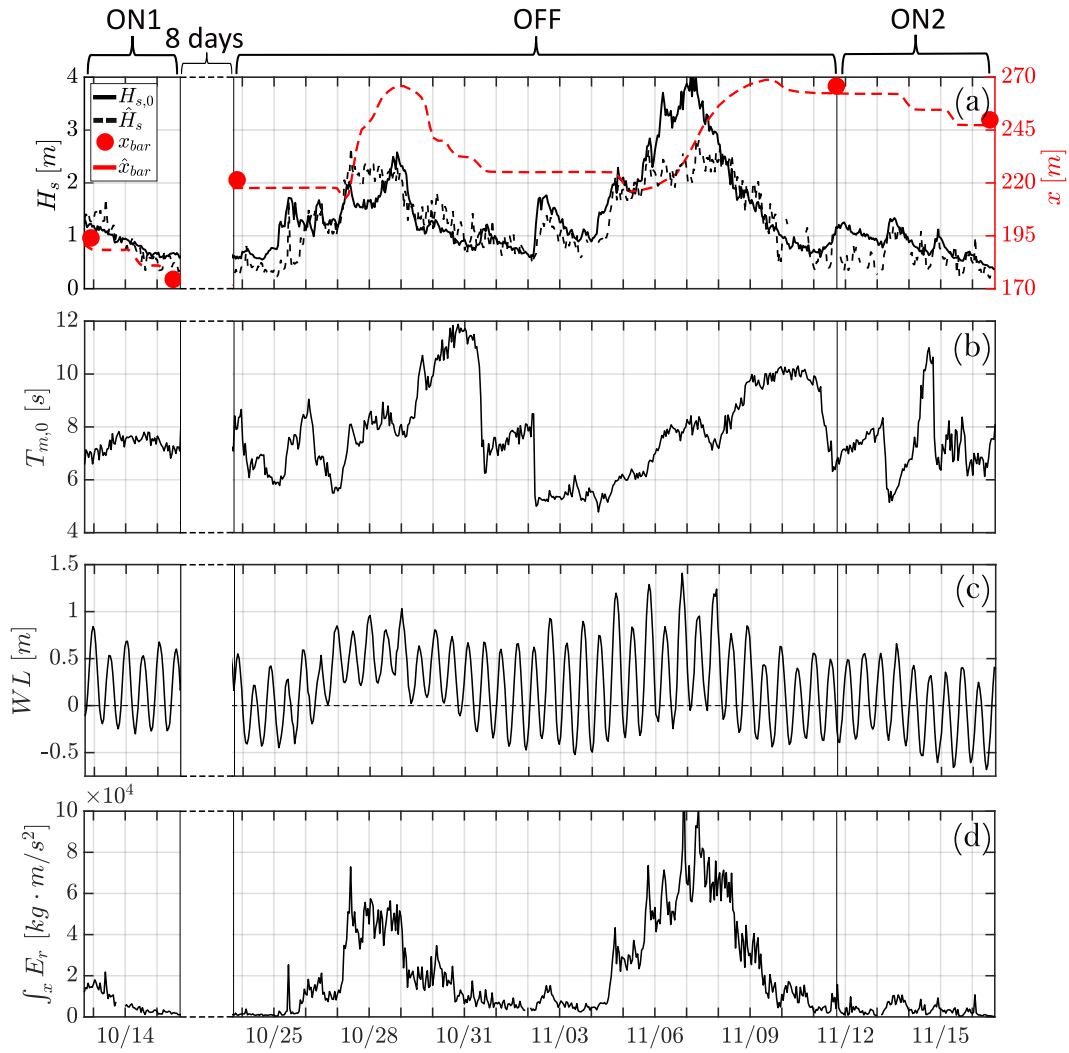

Figure 2. (a) Significant wave height (left-hand axis) observed in 17-m water depth (NDBC 44056, solid-black curve) and estimated by the radar at the outer edge of the surfzone (~4-m water depth, dashed-black curve), and the cross-shore locations of the crest of the sandbar (right-hand axis) from the surveys (solid-red circles) and corresponding model predictions (dashed-red curve), (b) mean period in 17-m water depth, (c) mean water level (relative to NAVD88, NOAA tide station 8651370 on the FRF pier, $y = 525$ m) and (d) cross-shore integrated roller energy estimated from the radar versus time (month/day) in 2021. Vertical black lines indicate the beginning of each of the 3 migration events. Data in the 8 days between the first and second event are omitted.

$$\hat{Q} = Q_c + Q_w + Q_s + Q_a \tag{1}$$

where transport is driven by mean currents (Q_c), wave-orbital velocity skewness (Q_w), bed-slope (gravity, Q_s), and orbital velocity asymmetry (Q_a). Vertical profiles of mean undertow currents are estimated with assumptions from the literature (Apotsos et al., 2007; Garcez-Faria et al., 2000), considering surface stress (Deigaard, 1993) and eddy viscosity (Reniers & Battjes, 1997), and accounting for a spatial lag in momentum transfer (Dubarbier et al., 2015; Reniers, Roelvink, & Thornton, 2004). Velocity skewness and asymmetry (Abreu et al., 2010) are estimated from the local Ursell number ($Ur = \frac{3H_s k}{8(kh)^3}$, where k is the wavenumber of the incident-wave centroidal frequency, and h is the water depth at each location along the cross-shore transect predicted by the morphological evolution model) (Doering & Bowen, 1995) using a fit to field data at several barred beaches (Ruessink et al., 2012). Standard parameters are employed in all terms (Dubarbier et al., 2015; Gallagher et al., 1998; Hoefel & Elgar, 2003; Hsu et al., 2006; Thornton et al., 1996), with a single set of calibration coefficients: $K_c = 0.0150$

for Q_c, $K_w = 0.0023$ for Q_w, $K_f = 0.0175$ for Q_s, and $K_a = 1.1200 \cdot 10^{-4}$ for Q_a (see Text S1 in Supporting Information S1 for details).

The evolution of the cross-shore profile is obtained from the estimated total transport every hour via the Exner equation:

$$\frac{\partial h}{\partial t} = -\frac{1}{\mu}\frac{\partial \hat{Q}}{\partial x} \tag{2}$$

where t is time and $\mu = 0.7$ accounts for the sediment concentration (packing) within the bed.

Three additional processes that have been shown to be important to sediment transport, but that typically have not been considered in energetics transport, are included here. Re-analysis of recent experiments (Grossmann, Hurther, Sánchez-Arcilla, & Alsina, 2023) indicated K_a is sensitive to wave bottom boundary layer dynamics near the bar, with larger values on the bar crest (parameterized here with the local Ursell number, Equation S29 in Supporting Information S1). Suspended sediment from breaking-wave injected turbulence (Christensen et al., 2019; Cox & Kobayashi, 2000; Larsen et al., 2020) was parametrized with an additional suspension velocity, $u_{inj}(x)$, in Q_c based on E_r at the surface and assuming exponential decay toward the bed (Equations S22 and S23 in Supporting Information S1). Energetics transport is depth-averaged, but the vertical extent of undertow-related suspended sediment transport (Gallagher et al., 1998; Grossmann, Hurther, van der Zanden, et al., 2023) was parametrized with a suspension elevation based on previously estimated suspended sediment profiles (Nielsen, 1986; Swart, 1974; Wilson et al., 2024) when calculating representative undertow (Equations S15–S19 in Supporting Information S1) and scaling transport in Q_c (Equation S25 in Supporting Information S1).

Model performance is evaluated by comparing the RMS prediction error E_{rms} between observed and predicted profiles at the end of events with Δ_{rms}, the rms change between profiles at the beginning and end of events to calculate the predictive skill, defined here as $1 - E_{rms}/\Delta_{rms}$ (Davis, 1976; Gallagher et al., 1998). If the model is perfect ($E_{rms} = 0$), then skill = 1. If the errors are as large as the observed changes, then skill = 0, and the model prediction is not better than a prediction that the profile at the end of the event equals the profile at the beginning. If the skill is negative, errors in the prediction are larger than the observed changes.

3. Results

In ON1 the observed 25-m onshore migration (compare solid-black with solid-red curve in Figure 3a) is replicated well (skill = 0.77) by the radar-driven sediment-transport and morphological change model (compare dashed-black with solid-black curve in Figure 3a) (see Movie S1 for a video of the simulation), with minor differences (the erosion offshore of the initial bar crest and the accretion near the final location of the crest are underpredicted slightly).

In OFF the observed 50-m offshore migration (compare solid-black with solid-red curve in Figure 3b) is predicted closely (skill = 0.60) (compare dashed-black with solid-black curve in Figure 3b) (see Movie S2 for a video of the simulation), although there is less erosion onshore of the bar ($150 < x < 240$ m) and less deposition offshore of the bar ($270 < x < 300$ m) than observed. Between the surveys, the model generates a sandbar (dashed-dotted green curve in Figure 3b) during the storm between 10/27 and 10/29 (Figure 2a). During subsequent calm conditions between 10/29 and 11/05 (Figure 2a) the model predicts that the bar migrated 50 m onshore (dotted-purple curve in Figure 3b). During the storm between 11/05 and 11/10 (Figure 2a) the model erodes the bar, transports its sediment offshore, and forms a distinct bar at a new location similar to that observed (compare dashed-black with solid-black curve near $x = 260$ m in Figure 3b).

In ON2 (Figure 3c), the observed 25-m onshore migration (compare solid-black with solid-red curve in Figure 3c) is modeled with skill = 0.50 (compare dashed-black with solid-black curve in Figure 3c) (see Movie S3 for a video of the simulation). Note that Δ_{rms} was small so that skill is low even though errors in the prediction (E_{rms}) are small.

Different terms in the transport equation (right-hand-side of Equation 1) were important during the 3 migration events (Figure 4). Onshore migration was forced by wave asymmetry, Q_a, and skewness, Q_w (Figures 4a and 4c). Asymmetry (red curves in Figures 4a and 4c) produced the largest transport, with maximum values on the onshore

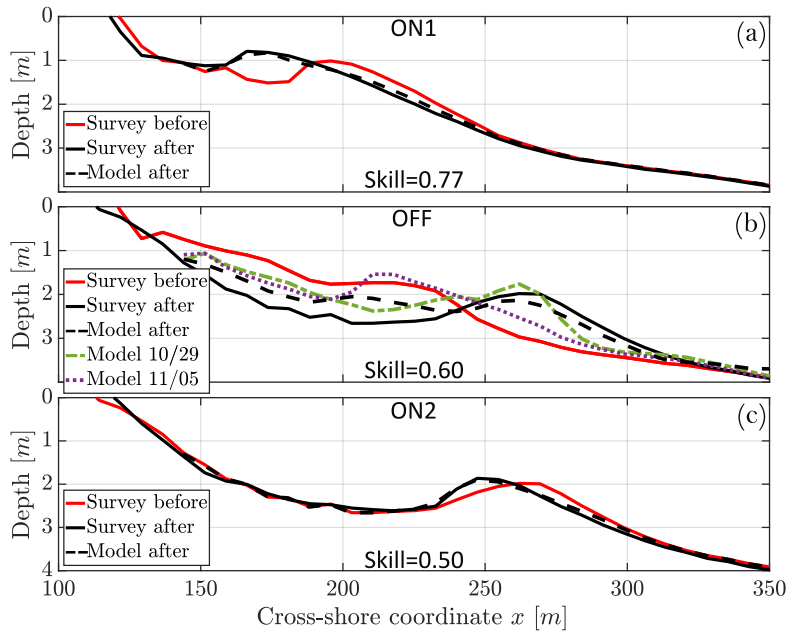

Figure 3. Seafloor depth (relative to the NAVD88 datum) versus cross-shore coordinate x observed at the start (solid-red curves) and end (solid-black curves) of each migration event, and predicted at the end of the migration by the model (dashed-black curves) for (a) ON1, (b) OFF, and (c) ON2. In addition, during the 20-day OFF event (panel (b)) model predictions also are shown of the formation of a bar after 5 days (dashed-dotted green curve) and its subsequent onshore migration after 12 days (dotted-purple curve), before offshore migration.

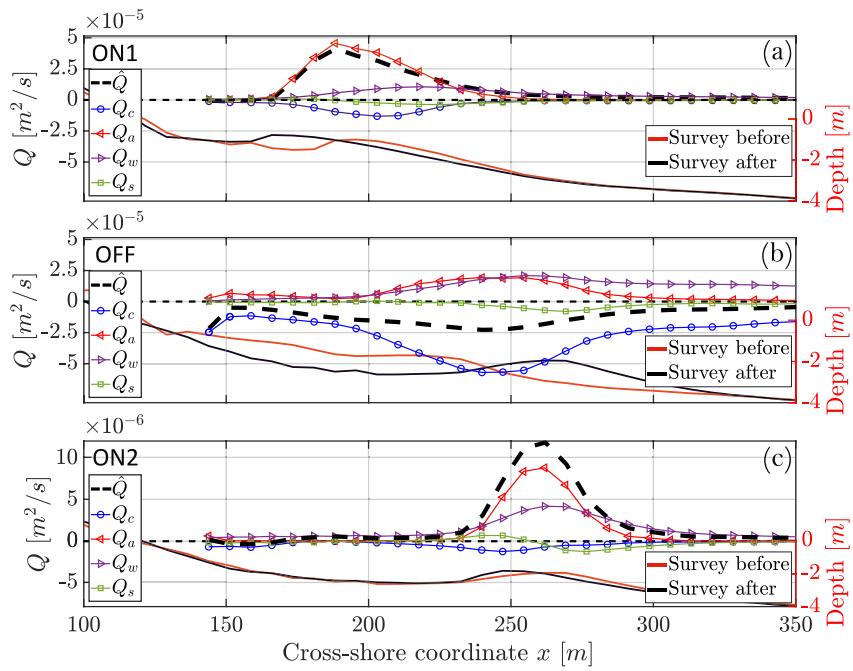

Figure 4. Model-estimated transport versus cross-shore coordinate x for (a) ON1, (b) OFF, and (c) ON2, with the total transport (dashed-black curves) used for updating morphology, and the current- (blue curves with circles), wave asymmetry- (red curves with left-facing triangles), wave skewness- (purple curves with right-facing triangles), and slope- (green curves with squares) driven transport terms. Note the different vertical scale for smaller transport in (c). Surveys of bathymetry are shown at the beginning (solid-red curves) and end (solid-black curves) of events (right-hand axes).

side of the initial bar crest location. Skewness (purple curves in Figures 4a and 4c) started increasing farther offshore (shoaling zone) and typically peaked on the offshore side of the bar. The undertow-related transport, Q_c (blue curves in Figures 4a and 4c) was relatively small for the low-energy waves ($H_{s,0} \leq 1$ m) during ON1 and ON2, but consistent with prior results (Rafati et al., 2021) balanced some of the wave-driven onshore transport. In the beginning of ON1 when $H_{s,0}$ was larger than 1 m (Figure 2a), at times the model predicted that undertow-driven offshore-directed transport deposited some sediment on the offshore slope of the bar (see Movie S1). However, asymmetry and skewness subsequently eroded the sediment and deposited it at the new bar position.

During larger wave heights ($H_{s,0} \geq 1.5$ m) the undertow-related offshore transport was dominant (blue curve in Figure 4b). From $x = 190$ to $x = 250$ m undertow forced net offshore transport to erode a bar trough during the first storm (10/27 to 10/29, Figure 2a) (see Movie S2). Farther offshore, the undertow-related transport decreased and was compensated by skewness- and asymmetry-driven onshore transport. This convergence of onshore and offshore transport led to formation of the bar visible on 10/29 (Figure 3b, dashed-dotted green curve). The subsequent onshore migration during small waves (10/29 to 11/04, Figure 2a) was forced by skewness- and asymmetry-driven transport, similar to the ON1 and ON2 (Figures 4a and 4c).

At the start of the second storm (11/05 to 11/08, Figure 2a) increasing wave heights eroded the crest of the bar and deposited sediment on its offshore slope (see Movie S2). This led to widening of the bar, producing a 70-m wide terrace in 2-m water depth on 11/08 without a clear bar crest. During large waves for another 2 days, a new trough was eroded onshore of $x = 250$ m and sediment was deposited at $250 \leq x \leq 300$ m through convergence of transport terms similar to the convergence during the first storm (10/27 and 10/29). Subsequently, 2 days of lower wave heights with net onshore transport produced a distinct bar shape (Figure 3b, dashed-black curve).

4. Discussion

The model results suggest that additional processes (terms) should be considered in energetics transport models. To evaluate the effects of these processes the model was re-run with terms deactivated (Figure 5). Ignoring the vertical extent of suspended sediment and using a depth-averaged undertow (Reniers, Thornton, et al., 2004) results in overestimation of the offshore transport when the bar migrated onshore (compare dash-dotted-dark-blue curves with the dashed-black curves in Figures 5a and 5c) (skill decreased by 0.49 and 0.24, respectively). Moreover, the offshore transport was underestimated when the bar migrated offshore (compare dash-dotted-dark-blue curve with the dashed-black curve in Figure 5b) (skill decreased by 0.2) resulting in a flattened profile without a bar. Without wave bottom boundary layer effects and using a cross-shore constant calibration of Q_a, onshore migration in ON1 was not predicted as well (compare dotted-red curve with the dashed-black curve in Figure 5a) (skill decreased by 0.17). In offshore event OFF (compare dotted-red curves with the dashed-black curves in Figure 5b) the lack of the bottom boundary layer term resulted in more deposition in the inner surf zone and less deposition offshore of the bar (skill decreased by 0.21). In contrast, the wave bottom boundary layer formulation had little effect on the simulation of bar migration in onshore event ON2 (compare dotted-red curve with the dashed-black curve in Figure 5c) (skill decreased by 0.01). Using a cross-shore constant, but increased coefficient of Q_a (not shown) incorrectly flattened the bar. Neglecting sediment suspended from injected turbulence had little effect on simulations of onshore migration (compare light-blue curves with circle markers with dashed-black curves in Figures 5a and 5c) (skill increased and decreased by 0.02, respectively), consistent with expectations during moderate waves ($H_{s,0} < 1.2$ m) where little turbulence is injected and may not reach the bed. However, suspended transport onshore of the offshore migrating bar (OFF) was reduced (compare light-blue curves with circle markers with dashed-black curves in Figure 5b), leading to underestimated erosion in the bar trough and underestimated deposition on the offshore side of the bar (skill decreased by 0.24), consistent with expectations under larger waves where turbulence injection does play a role.

Previous work (Dubarbier et al., 2015; Rafati et al., 2021; Ruessink et al., 2007, among others) used similar wave-averaged energy balances with (breaking) roller dissipation to simulate bar migration with comparable skill. In contrast to the present approach, those models input hydrodynamic information at the offshore boundary and estimate energy and momentum flux evolution throughout the nearshore using hydrodynamic coefficients calibrated to fit observed (or expected) wave height evolution. Simulation of observed morphological evolution required different coefficients (e.g., K_w, K_a) for onshore and offshore migration, as well as for different incident wave conditions (Dubarbier et al., 2015; Fernández-Mora et al., 2015; Kroon et al., 2025; Rafati et al., 2021). In

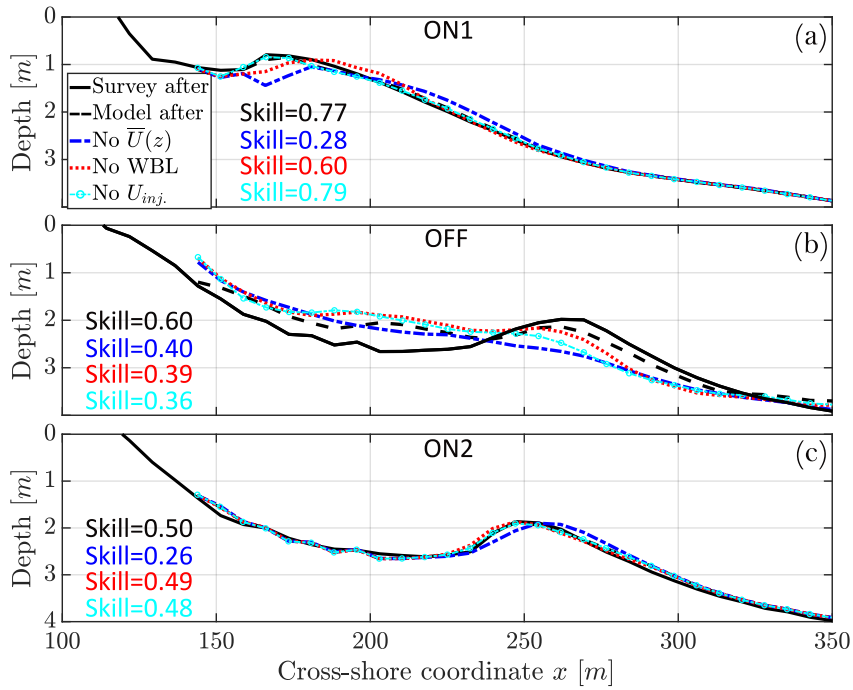

Figure 5. Seafloor depth versus cross-shore coordinate x from bathymetric surveys at the end of the migration event (solid-black curves) and model simulations considering all processes (dashed-black curves), with simplified undertow-related transport (dashed-dotted-dark-blue curves), without WBL effects in wave asymmetry-related transport (dotted-red curves), and without additional sediment suspension from breaking-injected turbulence (light-blue curves with circle markers).

contrast, here the same coefficients were used for all three events, with a cross-shore varying K_a to represent wave bottom boundary layer effects (improving results in two of the three events).

Obtaining accurate bathymetry is a major limitation in understanding nearshore processes, especially during storms (Salim & Wilson, 2021; Van Dongeren et al., 2008) when vehicles cannot be operated safely. Remote sensing approaches that estimate bar and trough locations from foam patterns (Guedes et al., 2011; Lippmann & Holman, 1990; Ruessink et al., 2009, among others) or that estimate bathymetry from wave celerity (Brodie et al., 2018; Lange et al., 2023, among others) are sensitive to changes in mean water levels (tides and surge) and wave conditions, and can have large errors for energetic waves. Meanwhile, numerical model predictions of bathymetric evolution based solely on offshore wave observations may have hydrodynamic (and thus subsequent morphologic) errors that accumulate with time. Many numerical models that include wave breaking parameterize the associated dissipation. The radar estimates of dissipation could be used to adjust the parameterizations so that the model dissipation is similar to the radar-estimated dissipation, thus providing a data-based constraint on the model estimates of dissipation. Additionally, a numerical model could be adapted to include radar estimates of dissipation directly. By enabling continuous concurrent estimates of the nearshore wave-breaking dissipation and bathymetry, the radar-driven model may lead to new understanding of the coupling and feedback between hydrodynamics and morphodynamics that lead to event-driven coastal evolution.

5. Conclusions

For the first time, radar measurements of wave energy dissipation at the ocean surface were used to estimate the hydrodynamics and sediment transport in the lower water column that drive nearshore morphological evolution. The calculations followed similar assumptions and formulations used in many other phase-averaged hydro-morphological models, but with waves and currents estimated from the radar and common parameterizations, rather than from a numerical model. Here, the radar estimated the dissipation of onshore propagating waves along a transect across the surfzone while a sand bar migrated 25 m onshore, 50 m offshore, and then 25 m back onshore in response to changing wave conditions over several weeks. Onshore transport processes included wave asymmetry-related onshore transport influenced by wave bottom boundary layer effects, whereas offshore

transport was influenced by the undertow-related vertical extent of sediment suspension. The results are consistent with previous studies of sandbar migration, suggesting wave nonlinearity is important to near-bottom transport during onshore migration in mild to moderate energy conditions and undertow-driven suspended sediment transport is important during offshore migration in energetic conditions.

Conflict of Interest

The authors declare no conflicts of interest relevant to this study.

Data Availability Statement

Data used here are available online. For bathymetry: https://chldata.erdc.dren.mil/thredds/catalog/frf/catalog.html, for incident wave conditions: https://www.ndbc.noaa.gov/stationhistory.php?station=44056, and for radar data see Streßer et al. (2025).

Acknowledgments
We thank Merrick Haller and the anonymous reviewer for their helpful comments and the field crews of the PVLAB and the FRF for obtaining observations in often difficult surfzone conditions. Funding was provided by the US National Science Foundation, the Doherty Foundation, and the Helmholtz Association through the "Changing Earth—Sustaining our Future" program.

References

Aagaard, T., Nielsen, J., & Greenwood, B. (1998). Suspended sediment transport and nearshore bar formation on a shallow intermediate-state beach. *Marine Geology*, *148*(3), 203–225. https://doi.org/10.1016/s0025-3227(98)00012-7

Abreu, T., Silva, P. A., Sancho, F., & Temperville, A. (2010). Analytical approximate wave form for asymmetric waves. *Coastal Engineering*, *57*(7), 656–667. https://doi.org/10.1016/j.coastaleng.2010.02.005

Apotsos, A., Raubenheimer, B., Elgar, S., Guza, R. T., & Smith, J. A. (2007). Effects of wave rollers and bottom stress on wave setup. *Journal of Geophysical Research*, *112*, C02003. https://doi.org/10.1029/2006JC003549

Bagnold, R. A. (1966). An approach to the sediment transport problem from general physics. In *Professional Paper 422-I U.S. Geological Survey*. US Government Printing Office.

Bailard, J. A. (1981). An energetics total load sediment transport model for a plane sloping beach. *Journal of Geophysical Research*, *86*(C11), 10938–10954. https://doi.org/10.1029/JC086iC11p10938

Battjes, J., & Janssen, J. (1978). Energy loss and set-up due to breaking of random waves. *Coastal Engineering*, *1978*, 569–587. https://doi.org/10.1061/9780872621909.034

Bowen, A. J. (1980). Simple models of nearshore sedimentation beach profiles and longshore bars. In S. B. McCann (Ed.), *The Coastline of Canada* (pp. 1–11). Geological Survey of Canada.

Brodie, K., Palmsten, M., Hesser, T., Dickhudt, P., Raubenheimer, B., Ladner, H., & Elgar, S. (2018). Evaluation of video-based linear depth inversion performance and applications using altimeters and hydrographic surveys in a wide range of environmental conditions. *Coastal Engineering*, *36*, 147–160. https://doi.org/10.1016/j.coastaleng.2018.01.003

Carini, R. J., Chickadel, C. C., Jessup, A. T., & Thomson, J. (2015). Estimating wave energy dissipation in the surf zone using thermal infrared imagery. *Journal of Geophysical Research: Oceans*, *120*(6), 3937–3957. https://doi.org/10.1002/2014JC010561

Catalán, P. A., Haller, M. C., Holman, R. A., & Plant, W. J. (2011). Optical and microwave detection of wave breaking in the surfzone. *IEEE Transactions on Geoscience and Remote Sensing*, *49*(6 PART 1), 1879–1893. https://doi.org/10.1109/TGRS.2010.2095864

Catalán, P. A., Haller, M. C., & Plant, W. J. (2014). Microwave backscattering from surf zone waves. *Journal of Geophysical Research: Oceans*, *119*(5), 3098–3120. https://doi.org/10.1002/2014jc009880

Chen, J., Raubenheimer, B., & Elgar, S. (2024). Wave and roller transformation over barred bathymetry. *Journal of Geophysical Research: Oceans*, *129*(5), e2023JC020413. https://doi.org/10.1029/2023JC020413

Chernyshov, P., Vrecica, T., Streßer, M., Carrasco, R., & Toledo, Y. (2020). Rapid wavelet-based bathymetry inversion method for nearshore X-band radars. *Remote Sensing of Environment*, *240*, 111688. https://doi.org/10.1016/j.rse.2020.111688

Christensen, D. F., Hughes, M. G., & Aagaard, T. (2019). Wave period and grain size controls on short-wave suspended sediment transport under shoaling and breaking waves. *Journal of Geophysical Research: Earth Surface*, *124*(12), 3124–3142. https://doi.org/10.1029/2019JF005168

Cox, D. T., & Kobayashi, N. (2000). Identification of intense, intermittent coherent motions under shoaling and breaking waves. *Journal of Geophysical Research*, *105*(C6), 14223–14236. https://doi.org/10.1029/2000jc900048

Dally, W. R., & Dean, R. G. (1984). Suspended sediment transport and beach profile evolution. *Journal of Waterway, Port, Coastal, and Ocean Engineering*, *110*(1), 15–33. https://doi.org/10.1061/(ASCE)0733-950X(1984)110:1(15)

Davis, R. E. (1976). Predictability of sea surface temperature and sea level pressure anomalies over the North Pacific Ocean. *Journal of Physical Oceanography*, *6*(3), 249–266. https://doi.org/10.1175/1520-0485(1976)006<0249:possta>2.0.co;2

Deigaard, R. (1993). A note on the three-dimensional shear stress distribution in a surfzone. *Coastal Engineering*, *20*(1–2), 157–171. https://doi.org/10.1016/0378-3839(93)90059-H

Díaz, H., Catalán, P. A., & Wilson, G. W. (2018). Quantification of two-dimensional wave breaking dissipation in the surf zone from remote sensing data. *Remote Sensing*, *10*(1), 38. https://doi.org/10.3390/rs10010038

Dibajnia, M., & Watanabe, A. (1992). Sheet flow under nonlinear waves and currents. *Coastal Engineering Proceedings*, *1*(23), 23. https://doi.org/10.9753/icce.v23

Doering, J. C., & Bowen, A. J. (1995). Parametrization of orbital velocity asymmetries of shoaling and breaking waves using bispectral analysis. *Coastal Engineering*, *26*(1–2), 15–33. https://doi.org/10.1016/0378-3839(95)00007-X

Dubarbier, B., Castelle, B., Marieu, V., & Ruessink, B. G. (2015). Process-based modeling of cross-shore sandbar behavior. *Coastal Engineering*, *95*, 35–50. https://doi.org/10.1016/j.coastaleng.2014.09.004

Dubarbier, B., Castelle, B., Ruessink, B. G., & Marieu, V. (2017). Mechanisms controlling the complete accretionary beach state sequence. *Geophysical Research Letters*, *44*(11), 5645–5654. https://doi.org/10.1002/2017GL073094

Duncan, J. H. (1981). An experimental investigation of breaking waves produced by a towed hydrofoil. In *Proceedings of the Royal Society of London. A. Mathematical and Physical Sciences* (Vol. 377, pp. 331–348). The Royal Society London. https://doi.org/10.1098/rspa.1981.0127

Dyhr-Nielsen, N., & Sørensen, T. (1970). Some sand transport phenomena on coasts wit bars. In *Proceedings of the 12th International Conference on Coastal Engineering* (Vol. 54, pp. 855–865). https://doi.org/10.1061/9780872620285.054

Farquharson, G., Frasier, S. J., Raubenheimer, B., & Elgar, S. (2005). Microwave radar cross sections and Doppler velocities measured in the surfzone. *Journal of Geophysical Research*, *110*(12), C12024. https://doi.org/10.1029/2005JC003022

Fernández-Mora, A., Calvete, D., Falqués, A., & de Swart, H. E. (2015). Onshore sandbar migration in the surfzone: New insights into the wave-induced sediment transport mechanisms. *Geophysical Research Letters*, *42*(8), 2869–2877. https://doi.org/10.1002/2014GL063004

Flores, R. P., Catalán, P. A., & Haller, M. C. (2016). Estimating surfzone wave transformation and wave setup from remote sensing data. *Coastal Engineering*, *114*, 244–252. https://doi.org/10.1016/j.coastaleng.2016.04.008

Frasier, S. J., & McIntosh, R. E. (1996). Observed wavenumber-frequency properties of microwave backscatter from the ocean surface at near-grazing angles. *Journal of Geophysical Research*, *101*(C8), 18391–18407. https://doi.org/10.1029/96JC01685

Frugier, S., Almar, R., Bergsma, E., & Granjou, A. (2025). SBI: A sandbar extraction spectral index for multi-spectral satellite optical imagery. *Coastal Engineering*, *200*, 104752. https://doi.org/10.1016/j.coastaleng.2025.104752

Gallagher, E. L., Elgar, S., & Guza, R. T. (1998). Observations of sand bar evolution on a natural beach. *Journal of Geophysical Research*, *103*(C2), 3203–3215. https://doi.org/10.1029/97JC02765

Garcez-Faria, A. F., Thornton, E. B., Lippmann, T. C., & Stanton, T. P. (2000). Undertow over a barred beach. *Journal of Geophysical Research*, *105*(C7), 16999–17010. https://doi.org/10.1029/2000JC900084

Grossmann, F., Hurther, D., Sánchez-Arcilla, A., & Alsina, J. M. (2023). Influence of the initial beach profile on the sediment transport processes during post-storm onshore bar migration. *Journal of Geophysical Research: Oceans*, *128*(4), e2022JC019299. https://doi.org/10.1029/2022JC019299

Grossmann, F., Hurther, D., van der Zanden, J., Sánchez-Arcilla, A., & Alsina, J. M. (2023). Near-bed sediment transport processes during onshore bar migration in large-scale experiments: Comparison with offshore bar migration. *Journal of Geophysical Research: Oceans*, *128*(3), e2022JC018998. https://doi.org/10.1029/2022JC018998

Guedes, R., Calliari, L., Holland, K., Plant, N., Pereira, P., & Alves, F. (2011). Short-term sandbar variability based on video imagery: Comparison between Time–Average and Time–Variance techniques. *Marine Geology*, *289*(1–4), 122–134. https://doi.org/10.1016/j.margeo.2011.09.015

Haller, M. C., & Catalán, P. A. (2009). Remote sensing of wave roller lengths in the laboratory. *Journal of Geophysical Research*, *114*(C7), C07022. https://doi.org/10.1029/2008JC005185

Hoefel, F., & Elgar, S. (2003). Wave-induced sediment transport and sandbar migration. *Science*, *299*(5614), 1885–1887. https://doi.org/10.1126/science.1081448

Holman, R., Plant, N., & Holland, T. (2013). cBathy: A robust algorithm for estimating nearshore bathymetry. *Journal of Geophysical Research: Oceans*, *118*(5), 2595–2609. https://doi.org/10.1002/jgrc.20199

Holman, R., & Stanley, J. (2007). The history and technical capabilities of Argus. *Coastal Engineering*, *54*(6–7), 477–491. https://doi.org/10.1016/j.coastaleng.2007.01.003

Horstmann, J., Bödewadt, J., Carrasco, R., Cysewski, M., Seemann, J., & Streßer, M. (2021). A coherent on receive X-band marine radar for ocean observations. *Sensors*, *21*(23), 7828. https://doi.org/10.3390/s21237828

Hsu, T.-J., Elgar, S., & Guza, R. T. (2006). Wave-induced sediment transport and onshore sandbar migration. *Coastal Engineering*, *53*(10), 817–824. https://doi.org/10.1016/j.coastaleng.2006.04.003

King, C. A. M., & Williams, W. W. (1949). The formation and movement of sand bars by wave action. *The Geographical Journal*, *113*, 70–85. https://doi.org/10.2307/1788907

King, D. B. (1991). *Studies in oscillatory flow bedload sediment transport. Doctoral Thesis*. University of California. Retrieved from https://escholarship.org/uc/item/491653vx

Kroon, A., Christiaanse, J. C., Luijendijk, A. P., de Schipper, M. A., & Ranasinghe, R. (2025). Parameter uncertainty in medium- term coastal morphodynamic modeling. *Scientific Reports*, *15*, 18471. https://doi.org/10.1038/s41598-025-02300-8

Lange, A., Fiedler, J., Merrifield, M., & Guza, R. (2023). UAV video-based estimates of nearshore bathymetry. *Coastal Engineering*, *185*, 104375. https://doi.org/10.1016/j.coastaleng.2023.104375

Larsen, B. E., van der Zanden, J., Ruessink, G., & Fuhrman, D. R. (2020). Stabilized RANS simulation of surfzone kinematics and boundary layer processes beneath large-scale plunging waves over a breaker bar. *Ocean Modelling*, *155*, 101705. https://doi.org/10.1016/j.ocemod.2020.101705

Lippmann, T., & Holman, R. (1990). The spatial and temporal variability of sand bar morphology. *Journal of Geophysical Research*, *95*(C7), 11575–11590. https://doi.org/10.1029/JC095iC07p11575

Miche, R. (1944). Mouvements ondulatoires de la mer. *Annales des Ponts et Chaussees*, *114*, 369–406.

Nielsen, P. (1986). Suspended sediment concentrations under waves. *Coastal Engineering*, *10*(1), 23–31. https://doi.org/10.1016/0378-3839(86)90037-2

Rafati, Y., Hsu, T. J., Elgar, S., Raubenheimer, B., Quataert, E., & van Dongeren, A. (2021). Modeling the hydrodynamics and morphodynamics of sandbar migration events. *Coastal Engineering*, *166*, 103885. https://doi.org/10.1016/j.coastaleng.2021.103885

Reniers, A. J. H. M., & Battjes, J. (1997). A laboratory study of longshore currents over barred and non-barred beaches. *Coastal Engineering*, *30*(1–2), 1–21. https://doi.org/10.1016/S0378-3839(96)00033-6

Reniers, A. J. H. M., Roelvink, J. A., & Thornton, E. B. (2004). Morphodynamic modeling of an embayed beach under wave group forcing. *Journal of Geophysical Research*, *109*, C01030. https://doi.org/10.1029/2002jc001586

Reniers, A. J. H. M., Thornton, E. B., Stanton, T. P., & Roelvink, J. A. (2004). Vertical flow structure during Sandy Duck: Observations and modeling. *Coastal Engineering*, *51*(3), 237–260. https://doi.org/10.1016/j.coastaleng.2004.02.001

Roelvink, J. A., & Stive, M. J. F. (1989). Bar-generating cross-shore flow mechanisms on a beach. *Journal of Geophysical Research*, *94*(C4), 4785–4800. https://doi.org/10.1029/JC094iC04p04785

Ruessink, B., Pape, L., & Turner, I. (2009). Daily to interannual cross-shore sandbar migration: Observations from a multiple sandbar system. *Continental Shelf Research*, *29*(14), 1663–1677. https://doi.org/10.1016/j.csr.2009.05.011

Ruessink, G., Bell, P. S., van Enckevort, I. M. J., & Aarninkhof, S. G. J. (2002). Nearshore bar crest location quantified from time-averaged X-band radar images. *Coastal Engineering*, *45*(1), 19–32. https://doi.org/10.1016/S0378-3839(01)00042-4

Ruessink, G., Kuriyama, Y., Reniers, A. J. H. M., Roelvink, J. A., & Walstra, D. J. R. (2007). Modeling cross-shore sandbar behavior on the timescale of weeks. *Journal of Geophysical Research*, *112*(F3), F03010. https://doi.org/10.1029/2006JF000730

Ruessink, G., Ramaekers, G., & van Rijn, L. C. (2012). On the parameterization of the free-stream non-linear wave orbital motion in nearshore morphodynamic models. *Coastal Engineering*, *65*, 56–63. https://doi.org/10.1016/j.coastaleng.2012.03.006

Salim, A., & Wilson, G. (2021). Validation and analysis of a 1-D variational assimilation scheme for bathymetry inversion. *Coastal Engineering*, *167*, 103895. https://doi.org/10.1016/j.coastaleng.2021.103895

Stive, M. J. F., & Wind, H. G. (1986). Cross-shore mean flow in the surfzone. *Coastal Engineering*, *10*(4), 325–340. https://doi.org/10.1016/0378-3839(86)90019-0

Streßer, M., Collins, C. O. I., Lund, B., Humbertson, J., Horstmann, J., Carrasco, R., et al. (2024). *Coherent marine X-band RadarDeployment during DUNEX (Techreport No. ERDC/CHL TR-24-16)*. US Army Engineer Research and Development Center, Coastal and Hydraulics Laboratory. https://doi.org/10.21079/11681/49218

Streßer, M., Grossmann, F., Raubenheimer, B., & Elgar, S. (2025). Radar-derived roller quantities used in "Radar estimates of surfzone dissipation drive a morphological evolution model" [Dataset]. *Zenodo*. https://doi.org/10.5281/zenodo.17130491

Streßer, M., Horstmann, J., & Bascheck, B. (2022). Surface wave and roller dissipation observed with shore-based Doppler marine radar. *Journal of Geophysical Research: Oceans*, *127*(8), e2022JC018437. https://doi.org/10.1029/2022JC018437

Streßer, M., Seemann, J., Carrasco, R., Cysewski, M., Horstmann, J., Baschek, B., & Deane, G. (2021). On the interpretation of coherent marine radar backscatter from surf zone waves. *IEEE Transactions on Geoscience and Remote Sensing*, *60*, 1–14. https://doi.org/10.1109/TGRS.2021.3103417

Svendsen, I. A. (1984). Mass flux and undertow in a surfzone. *Coastal Engineering*, *8*(4), 347–365. https://doi.org/10.1016/0378-3839(84)90030-9

Swart, D. H. (1974). *Offshore sediment transport and equilibrium beach profiles. PhD Thesis*. Delft Hydraulics. Retrieved from https://resolver.tudelft.nl/uuid:057cb136-5f5b-484a-878d-5616fbaeda4e

Thornton, E. B., & Guza, R. T. (1983). Transformation of wave height distribution. *Journal of Geophysical Research*, *88*(C10), 5925–5938. https://doi.org/10.1029/JC088iC10p05925

Thornton, E. B., Humiston, R., & Birkemeier, W. (1996). Bar/trough generation on a natural beach. *Journal of Geophysical Research*, *101*(C5), 12097–12110. https://doi.org/10.1029/96JC00209

Valenzuela, G. R. (1978). Theories for the interaction of electromagnetic and oceanic waves—A review. *Boundary-Layer Meteorology*, *13*(1), 61–85. https://doi.org/10.1007/BF00913863

Van Dongeren, A., Plant, N., Cohen, A., Roelvink, D., Haller, M. C., & Catalán, P. (2008). Beach Wizard: Nearshore bathymetry estimation through assimilation of model computations and remote observations. *Coastal Engineering*, *55*(12), 1016–1027. https://doi.org/10.1016/j.coastaleng.2008.04.011

van Rijn, L. C., Tonnon, P. K., & Walstra, D. J. R. (2011). Numerical modelling of erosion and accretion of plane sloping beaches at different scales. *Coastal Engineering*, *58*(7), 637–655. https://doi.org/10.1016/j.coastaleng.2011.01.009

Wijnberg, K., & Kroon, A. (2002). Barred beaches. *Geomorphology*, *48*(1), 103–120. https://doi.org/10.1016/S0169-555X(02)00177-0

Wilson, G. W., Dickhudt, P., & Aldrich, J. (2024). Sediment dynamics in the energetic nearshore zone: Acoustic remote sensing and model validation. *Journal of Geophysical Research: Oceans*, *129*(10), e2024JC021563. https://doi.org/10.1029/2024JC021563

Wu, Y., Zhang, Q., Liu, Z., & Ji, C. (2025). Experimental investigation on wave roller area evolution in the surf zone. *Applied Ocean Research*, *155*, 104460. https://doi.org/10.1016/j.apor.2025.104460

References From the Supporting Information

Deigaard, R., & Fredsøe, J. (1989). Shear stress distribution in dissipative water waves. *Coastal Engineering*, *13*(4), 357–378. https://doi.org/10.1016/0378-3839(89)90042-2

Drake, T. G., & Calantoni, J. (2001). Discrete particle model for sheet flow transport in the nearshore. *Journal of Geophysical Research*, *106*(C9), 19859–19868. https://doi.org/10.1029/2000JC000611

Kumar, N., Voulgaris, G., Warner, J. C., & Olabarrieta, M. (2012). Implementation of the vortex force formalism in the coupled ocean-atmosphere-wave-sediment transport (COAWST) modeling system for inner shelf and surfzone applications. *Ocean Modelling*, *47*, 65–95. https://doi.org/10.1016/j.ocemod.2012.01.003

Martins, K., Blenkinsopp, C., Deigaard, R., & Power, H. E. (2018). Energy dissipation in the inner surfzone: New insights from lidar-based roller geometry measurements. *Journal of Geophysical Research: Oceans*, *123*(5), 3386–3407. https://doi.org/10.1029/2017jc013369

Nairn, R. B., Roelvink, J. A., & Southgate, H. N. (1991). Transition zone width and implications for modelling surfzone hydrodynamics. In B. L. Edge (Ed.), *Proceedings of the 22nd Coastal Engineering International Conference 1990* (pp. 68–82). American Society of Civil Engineers.

Nielsen, P. (1992). Coastal bottom boundary layers and sediment transport. *Advanced Series on Ocean Engineering*, *4*. https://doi.org/10.1142/1269

Okayasu, A., Shibayama, T., & Mimura, N. (1986). Velocity field under plunging waves. *Coastal Engineering Proceedings*, *1*(20), 50. https://doi.org/10.9753/icce.v20.50

Svendsen, I. A. (2005). Introduction to nearshore hydrodynamics. *World Scientific*, *24*. https://doi.org/10.1142/5740

Uchiyama, Y., McWilliams, J. C., & Shchepetkin, A. F. (2010). Wave—Current interaction in an oceanic circulation model with a vortex-force formalism: Application to the surfzone. *Ocean Modelling*, *34*(1–2), 16–35. https://doi.org/10.1016/j.ocemod.2010.04.002

Zhang, C., Zhang, Q., Zheng, J., & Demirbilek, Z. (2017). Parameterization of nearshore wave front slope. *Coastal Engineering*, *127*, 80–87. https://doi.org/10.1016/j.coastaleng.2017.06.008